Korean Chem. Eng. Res., 61(2), 287-295 (2023)
https://doi.org/10.9713/kcer.2023.61.2.287
PISSN 0304-128X, EISSN 2233-9558

Fe-Nanoparticle Amalgamation Using *Lagenaria siceraria* Leaf Aqueous Extract with Focus on Dye Removal and Antibacterial Efficacy

Kirti*, Suantak Kamsonlian*,†, Vishnu Agarwal, Ankur Gaur* and Jin-Won Park*****

**Department of Chemical Engineering, Motilal Nehru National Institute of Technology Allahabad, Prayagraj - 211004, India*
***Department of Biotechnology, Motilal Nehru National Institute of Technology Allahabad, Prayagraj - 211004, India*
****Department of Chemical and Biomolecular Engineering, Yonsei University, 262 Seoul, 03722, Korea*
(Received 16 August 2022; Received in revised from 7 November 2022; Accepted 15 November 2022)

Abstract – Iron nanoparticles (Fe-NPs) were synthesized employing *Lagenaria siceraria* (LS) leaf aqueous extract as a reducing and capping medium to remove methylene blue (MB) dye and have antibacterial properties against G-negative (Escherichia coli) and G-positive bacteria (Staphylococcus aureus). The formation of LS-Fe-NPs (*Lagenaria-siceraria*-iron-nanoparticles) was confirmed by a change in color from pale yellow to dark brown. Characterization techniques, such as particle size analysis (PSA), transmission electron microscopy (TEM) and scanning electron microscopy (SEM), were employed to prove nano spherical particles of size range between 80-100 nm. Phytochemicals and the presence of iron in LS-Fe-NPs nanoparticles were proved by UV-visible spectrophotometry. Further, Fourier transform infrared spectroscopy (FTIR) analysis results confirmed the existence of bioactive molecules in the plants. The magnetic property was analyzed using a vibrating sample magnetometer (VSM), which displayed that the synthesized nanoparticles were superparamagnetic and exhibiting a saturation magnetization of 12.5 emu/g. Synthesized magnetic nanoparticles were used in methylene blue (MB) dye removal through adsorption. About 83% of 100 mg/L MB dye was removed within 120 min at pH 6 with a maximum adsorption capacity of 246.8 mg/g. Antibacterial efficacy of LS-Fe-NPs was screened against G-negative (Escherichia coli) and G-positive bacteria (Staphylococcus aureus), respectively, and found that LS-Fe-NPs were effective against Staphylococcus aureus.

Key words: Nanoparticles, Bioactive molecules, LS-Fe-NPs, Methylene blue, Adsorption, Antibacterial

1. Introduction

Limited freshwater supply and water pollution issues have become increasingly common throughout the world [1]. Unfortunately, nearly 3.1 percent of deaths occurring every single year, which amounts to around 1.7 million people around the world, are attributed to hazardous potable water [2]. It is anticipated that more than 57 percent of the worldwide population will face water scarcity by year 2050 [3]. Shortage of drinking water is mainly due to contamination. Dangerous organic and inorganic contaminants discharging from industries are poisoning the water of developing countries [4]. The first pollutant visible in wastewater is color. Dyes are extensively utilized in numerous industries, such as plastics, pulp and paper, textiles, leather. Textile effluent has been identified as one of the largest sources of wastewater in ASEAN countries. Azo dyes are a class of organic compounds with a complex aromatic molecular configuration that can impart vivid color to different compounds. On the other hand, the dye molecules due to aromatic complex structures make them long-lasting and less volatile [5]. Another key concern is hazardous bacteria found in water, such as Escherichia coli (diarrhea), Vibrio cholerae (cholera), Salmonella typhosa (typhoid), and others. This necessitates the urgent need for technological progress in order for fast and effective elimination of pollutants and toxins from aquatic ecosystems [6].

Nanotechnology leads to the creation of new materials or the renovation of existing materials. The primary objective of nanotechnology is synthesizing nanoparticles, which have a wide scope of use in numerous science disciplines [7,8]. Among various nanoparticles, iron-oxide magnetic nanoparticles (IOMNPs) have numerous applications in fields like drug delivery [9,10], magnetics targeting [11], hyperthermia cancer therapy [12,13], biomolecule separation [14,15], stem cell sorting and manipulation, thermal-ablation [16], negative MRI contrast enhancement, gene therapy [17], applications in food-industry [18] and bioprocess intensification antimicrobial agents [19]. Furthermore, because their surface sites are more inherently susceptible to colored compounds, heavy metals and other pollutants, magnetic nanoparticles have been widely used for organic or inorganic contaminated wastewater treatment [20,21]. There is already a plethora of chemical, physical, hybrid, and biological techniques accessible to synthesize various types of nanoparticles [22]. Each approach produces nanoparticles with distinct features. The co-precipitation method is perhaps the easiest and most effective way to obtain magnetic particles chemically. The key benefit of the co-precipitation method is that it can produce a large amount of nanoparticles [23,24]. The technology of synthesizing green NPs

† To whom correspondence should be addressed.
E-mail: suantakk@mnnit.ac.in

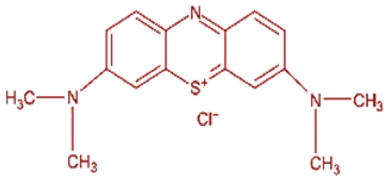

Fig. 1. Structure of methylene blue (MB) dye, the molecular formula is $C_{16}H_{18}N_3SCl$ and molecular weight is 319.85 g/mol, IUPAC name 3,7-bis (dimethylamino)-phenothiazine-5-ium chloride.

has received significant attention, and it focuses on techniques to reduce the use of hazardous compounds to save the environment [25]. The synthesis of green metallic NPs is the reduction and oxidation process that takes place because of the reduced capacity of extracellular or intracellular components like carbohydrates, phenols, proteins, metabolites and other organic acids, which provide electrons to the metal cations, convert them into a metallic form having zero charge and on a nanometer size [26]. Aldehydes, alcohols, carboxyl, ketones, amines, sulfhydryl and hydroxyl are the intermediate functional groups in the production of NPs, hence nearly any biological substance that contains these groups may be used to convert metal ions into NPs [27].

There is no literature available on the implementation of *Lagenaria siceraria* aqueous extract along with magnetic nanoparticles in the dye removal application. In the present study, *Lagenaria siceraria* leaves were employed for the synthesis of Fe-NPs by the green route. *Lagenaria siceraria* is a tropical and subtropical annual non-woody herbaceous climber plant having an ancient history of conventional medicinal usage in various countries. The entire plant has been proven to be useful in ancestral medical systems. The fruit is diuretic and sweet, antibilious, antipyretic, tonic for the liver, antiperiodic and vulnerary. It can treat blood illnesses, as well as muscle discomfort and also it is useful in the treatment of various diseases, such as jaundice, hypertension, diabetes, ulcers, congestive cardiac failure, piles, colitis, insanity and dermis problems [28]. In the leaf, phenolics, flavonoids and tannins are present. The phytochemicals that have carboxyl, hydroxyl, and functional amino groups, can be used as metal-capping medium and reducing medium to synthesize Fe-NPs [29]. Nanoparticles synthesized from *Lagenaria siceraria* leaves aqueous extract which are super-paramagnetic in nature have been used in this study to remove MB dye (structure of MB dye is shown in Fig. 1) from synthetic water via adsorption technique. The antibacterial activity is also assessed against G-negative (Escherichia coli) and G-positive bacteria (Staphylococcus aureus).

2. Materials and Methods

2-1. Materials

The chemicals used in the present work are from certified reagent grade that have not been subjected to any additional treatment. Distilled water was used to prepare the solutions. Volumetric flasks made of glass and the reaction vessels were treated with 10% H_2SO_4 (Merck India) and rinsed multiple times. Methylene blue dye (MB) was purchased from Sigma Aldrich, used as adsorbate. Ferric sulfate heptahydrate ($Fe_2SO_4.7H_2O$, 99.5%), sodium hydroxide (NaOH), hydrochloric acid (HCL) and ethanol (99.9%) were purchased from Merck India used in this investigation.

2-2. Synthesis of LS-Fe-NPs

Fresh *Lagenaria siceraria* leaves were obtained from a home garden. *Lagenaria siceraria* (LS) leaves were gently cleaned with distilled water to remove surface dust. Fig. 2 represents the detailed process of nanoparticle synthesis. The extract was made by boiling 100 g finely chopped fresh *Lagenaria siceraria* leaves in 500 mL

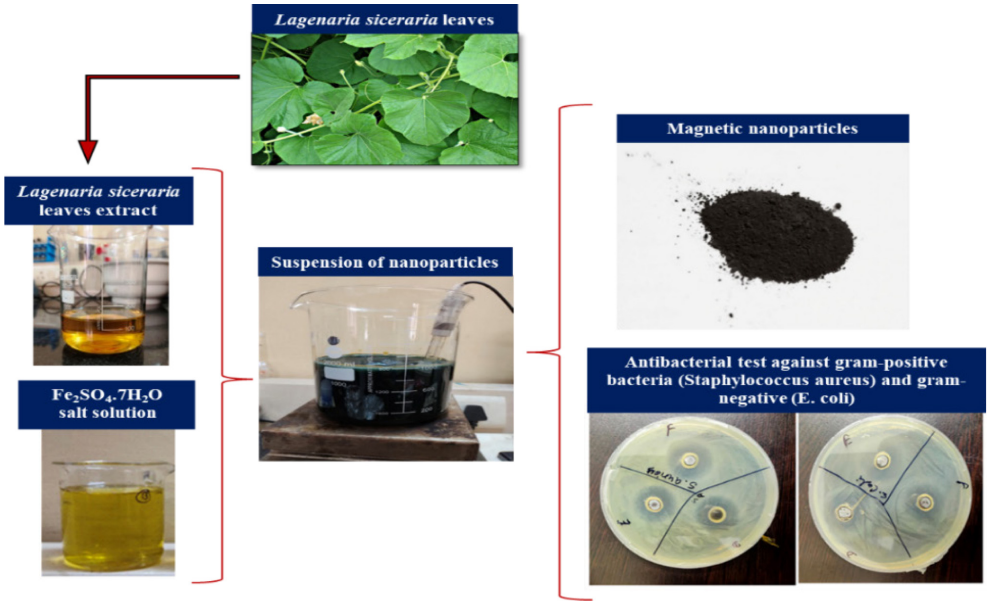

Fig. 2. Process details for synthesis of nanoparticles (LS-FE-NPs).

distilled water (60℃) for 1.5 h; after that the obtained extract of the plant was left to reach room temperature, then filtration was done in vacuum and the obtained solution was stored in a refrigerator at 4 ℃ for further use. The co-precipitation method was used to prepare nanoparticles. The nanoparticles were synthesized with some modifications as described by Wang et al., 2014 [30]. The leaf extract was added to 0.06 M $Fe_2SO_4.7H_2O$ precursor salt solution with a volume ratio of 2:1 and constant stirring was done for 1hr. The color of suspension changed from pale yellow to a dark brown color, which was an indication of the reduction of Fe-ions. Dropwise addition of 0.01 M of NaOH was done for precipitation. Diluted HCL was also added dropwise until the pH 10 was obtained. After this, the suspension was put for precipitation for about 30 min. The suspension was then centrifuged for 15 minutes at 5000 RPM to separate the nanoparticles. Proper washing of obtained NPS with distilled water and ethanol was done several times followed by centrifugation until the pH 7 was attained. Before use, the NPs were dried using the vacuum at 40 ℃ for 24 h and stored in sample holder.

2-3. Characterizations

For the examination of morphological attributes SEM analysis was carried out. Fig. 2 indicates the successful synthesis of nanoparticles. The samples were taped to metallic discs and then enclosed with a thin gold layer that was electrically conductive and were analyzed under SEM modal Instrument JSM-6380 installed at Visvesvaraya National Institute of Technology, Nagpur (India). For morphological characteristics, scanning electron microscopy was employed for 4 min at a 5 kV accelerating voltage upon gold coating [31]. The pictures were taken at different magnifications. The presence of different elements in the NPs was estimated using energy dispersive X-ray analysis (EDS) in conjunction with SEM. The sample was evaluated using EDS software, which performed ZAF correction and subsequent peak combination to get the exact quantity of the components that occurred in the specimen. To examine the size of the nanoparticles, TEM (200 kV, HITACHI H-800, Japan) and PSA (Microtrac\FLEX 11.0.0.4, Japan) techniques were employed. PSA has been done which was installed at MNNIT Allahabad, Uttar Pradesh. FTIR spectra of the green LS-Fe-NPs show the various phytochemicals present on the NP's surface. For measurement, 1% (w/w) sample was combined with 100 mg KBr powder and pressed into a sheer slice. FTIR was done from Material Research Center MNIT, Jaipur of model name Perkin Elmer Spectrum version 10.4.00. UV-vis spectroscopy is a quantitative measurement used to determine the concentration LS-Fe-NPs. UV-Vis-spectrometer (Perkin Elmer, Shimadzu, Japan) installed at the Chemical Engineering Department, MNNIT Allahabad, Uttar Pradesh, was used with reference to distilled water was found in the range of 200-600 nm. VSM is a scientific tool that determines magnetic properties and magnetic behavior of synthesized NPs. VSM was done from CIR Lab, MNNIT Allahabad, Uttar Pradesh of model name Versa Lab VSM version 2.0,1.0.

2-4. Dye adsorption experiment

Erlenmeyer flasks were used for all of the batch adsorption studies. For adsorption, a 100 mL aqueous solution of MB dye (100 mg/L) was put in the flask, along with a known amount of prepared iron nanoparticles and then the flask was put on a magnetic stirrer at 150 RPM for 120 min at room temperature (25 ℃) and pH 6. The flask was then removed from the stirrer and iron obtained iron nanoparticles was separated by a magnetic bar and the leftover MB dye concentration in the solution was measured using a UV-Visible spectrophotometer (Systronics 117) with a wavelength of 664 nm. The percentage of MB dye removal was computed from Eq. (1):

$$\% \text{ Removal} = \frac{(C_i - C_e)}{C_i} \times 100 \tag{1}$$

The equilibrium adsorption capacity was computed using Eq. (2):

$$q_e = \frac{(C_i - C_e)}{m} \times V \tag{2}$$

where, q_e = Adsorption capacity at equilibrium (mg/g)

C_i and C_e = Initial and equilibrium adsorbate concentration (mg/L), respectively

m = Adsorbate mass (g)

V = Volume of the solution (L)

Control was prepared simultaneously using 100 mg/L of MB and its concentration was measured in UV Visible Spectrophotometer (Motras Scientific UV PLUS, India) after each adsorption experiment. Different parameters (pH, adsorbent dose, Initial concentration and contact time) were adjusted to find the optimum conditions for MB adsorption bye adjusting one parameter at a time while maintaining the others constant. The pH of dye was varied (2, 4, 6 and 10), dose of iron nanoparticles was varied from 2 mg/L to 8 mg/L, the starting concentration of MB was varied from 100 mg/L to 500 mg/L, the contact time of adsorbent and adsorbate was from 5 min to 120 min.

2-5. Antibacterial activity

The Agar disc plate method was used to determine the LS-Fe-NPs suspension which has antibacterial action against S-aureus, which is a g-positive bacteria and g-negative bacteria, Escherichia coli, it was cultured in an agar nutrient medium before being used. The medium was autoclave-sterilized at 120 ℃ for 30min. Microorganism colloidal solution (52.20 CFU/L, McFarland barium sulfate standard) was cultured for 40~50 ℃ (0.50/50 mL medium) and then transferred to a Petri dish. Before being placed in the nanomaterial solutions, dual bacteria were placed separately within the broth solution, which was distributed across different tubes and thoroughly assembled in the center of the Petri dish. Both bacteria were placed in broth solution in discrete test tubes, then a well was created in the Petri dish's center and filled with LS-Fe-NPs solution. For antibacterial properties, bacterial growth was detected after the above plates were pre-incubated for 24 h at 37 ℃. The distance

between the disk's border and the edge of the bacterial growth was used to calculate the appearance of inhibition zones [17].

3. Results and Discussion

3-1. Characterization by SEM and EDX

Fig. 3(a) and (b) show the sizes and morphology of LS-Fe-NPs. The NPs exhibit a spherical shape having non-uniform features in agglomerated form. This aggregation could be explained by the presence of polyphenols and antioxidants in *Lagenaria siceraria* leaves extract serving as a capping medium on the surface of particles [16]. The product's constitution was also determined by EDS as shown in Fig. 4. The EDX spectra revealed a high peak of iron in the 6.0~7.0 keV band. The oxygen was also found in the energy range from 1.0 to 2.0 keV. The obtained results show a total element's content of 61.92 wt% Fe, 36.08 wt% O and other trace elements like 1.7 wt% Pt and 0.3 wt% S were present.

3-2. Characterization by TEM and PSA

The size distribution of the prepared nanoparticles was determined using TEM. Fig. 5 shows that LS-Fe-NPs are spherical shape having a size of 100 nm, while PSA analysis confirmed that they were in the nano range. TEM investigation was carried out using a 200 kV HITACHI H-800 service. Similar findings were reported by Katata-Seru et al., 2018 [32] by depicting FeNPs spherical shape of nanoparticles prepared from Moringa oleifera extracts. The differential intensity

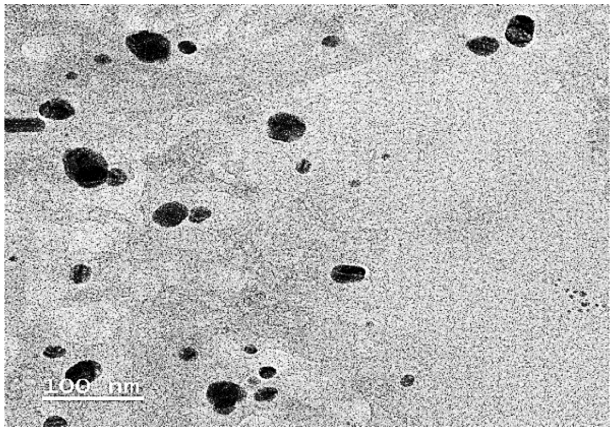

Fig. 5. TEM image of synthesized LS-Fe-NPs.

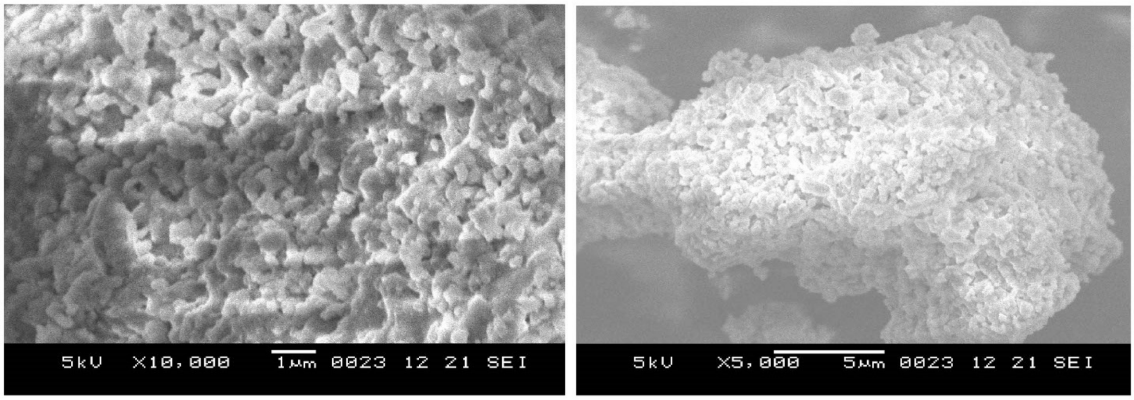

Fig. 3. SEM image of LS-Fe-NPs at different magnifications: (a) 10000 and (b) 5000.

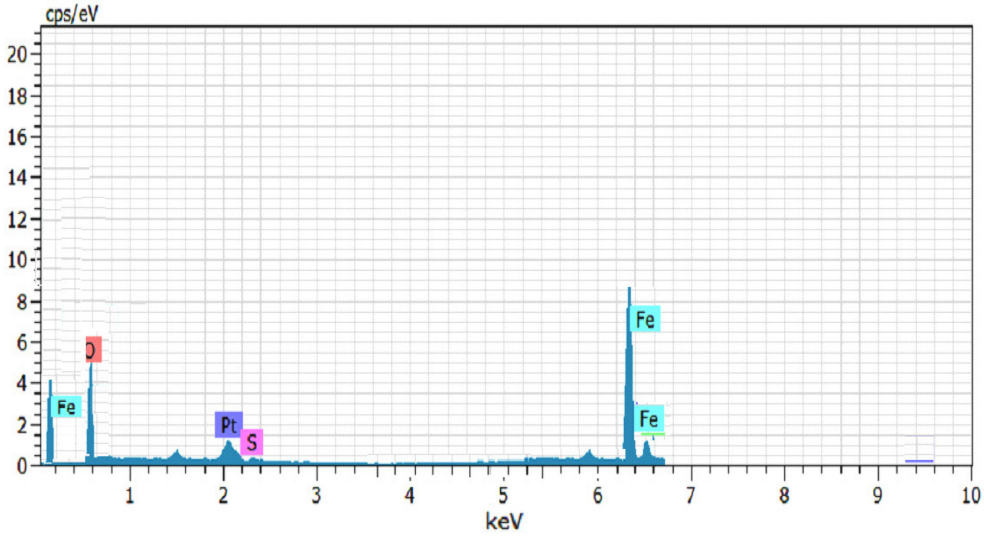

Fig. 4. EDX spectrum of LS-Fe-NPs.

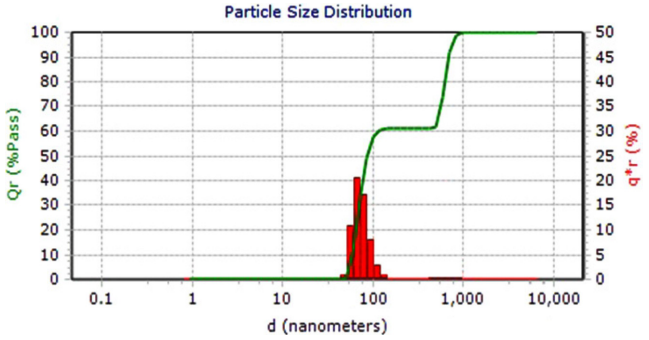

Fig. 6. Particle size distribution (PSA) image synthesized LS-Fe-NPs.

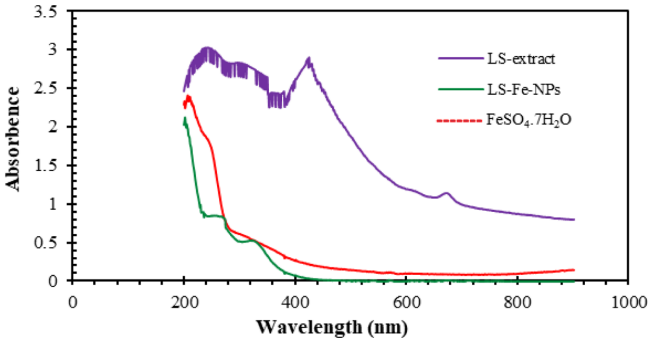

Fig. 7. UV-vis spectrum of *Lagenaria siceraria* leaf extract, $FeSO_4 \cdot 7H_2O$ precursor salt and iron nanoparticles.

related to particle size distributions of the synthesized LS-Fe-NPs obtained from PSA analysis is shown in Fig. 6, which shows that the particles are of nano-size in approximately 80~100 nm range. Similar results were also reported in literature [31].

3-3. Characterization by UV-Visible spectroscopy

Fig. 7 shows the UV spectra of *Lagenaria siceraria* leaf extract, $FeSO_4 \cdot 7H_2O$ precursor salt and iron nanoparticles. The peaks at 245-304 nm in leaf extract belong to polyphenols, according to UV spectra [33]. However, after reaction with Fe^{2+}, the intensity of peak 272 nm decreased, and the production of LS-Fe-NPs was observed in wide absorption at a higher wavelength. The function of the phytochemical-rich Lagenaria siceraria extract in the nanoparticle formation process was revealed by the change in color from pale yellow to dark brown (Fig. 2). UV-vis absorption spectra of an aqueous solution of the *Lagenaria siceraria* extract were observed in both the absence and existence of Fe^{2+}. From the figure it is clear that the absorbance of *Lagenaria siceraria* extract is considerably changed and interacts with the Fe^{2+}. The absorbance peak at 273-301 nm indicates the formation of iron oxide nanoparticles [34].

3-4. Characterization by FT-IR

To investigate the capping agents on the LS-Fe-NPs surface and detect the iron oxide forms, FTIR analysis of prepared iron nanoparticles was used, which is shown in Fig. 8. To confirm the phytochemicals accountable for the precursor metal salt reduction and capping of

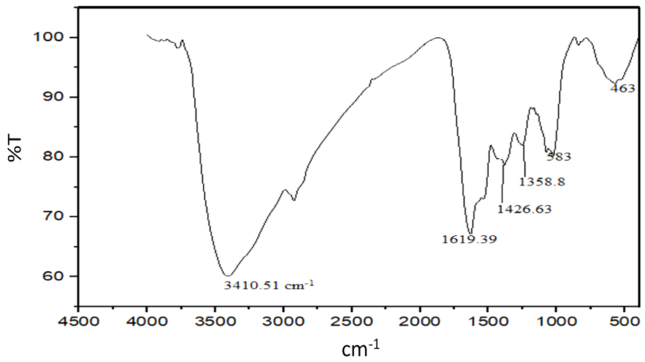

Fig. 8. FTIR spectra of synthesized LS-Fe-NPs.

Fe-NPs, 3500 cm^{-1} to 3200 cm^{-1} shows the OH polyphenolic group's vibrational stretching of *Lagenaria siceraria*, at a specific band at 3410.51 cm^{-1}. A band at 1619.39 cm^{-1} is attributed to aromatic ring deformation or stretching vibrations of C=C and -C=O groups [35]. The Fe=O stretching and bending vibration modes of iron oxide are assigned to the IR bands at 583 cm^{-1}, and 463 cm^{-1}, respectively [36]. A narrow peak at 1426.63 cm^{-1} and 1358.80 cm^{-1} in the sample was attributed to NO^{-3} from residual nitrate ions [22]. The very narrow band at 1720 cm^{-1} in LS extract represents carbonyl groups produced from dimerized saturated aliphatic acids. The appropriate adsorption bands at wave numbers (<700 cm^{-1}) were produced from vibrations of Fe-O bonds of iron oxide. The existence of organic groups on the surface of iron oxide nanoparticles may increase their hydrophobicity, making them more suitable for use in hydrophobic fluids while also avoiding aggregation of nanoparticles [37].

3-5. Characterization by VSM

The magnetic characteristics of LS-Fe-NPs were evaluated using VSM at ambient temperature in the field range of 6 KOe to measure the magnetization against the applied magnetic field (M–H) curve. Fig. 9 shows the magnetization of LS-Fe-NPs as a function of the applied magnetic field at 298 K. With an increase in the magnetic field, the magnetization also increased. The electromagnetic characteristics of nanoparticles were characterized by factors such

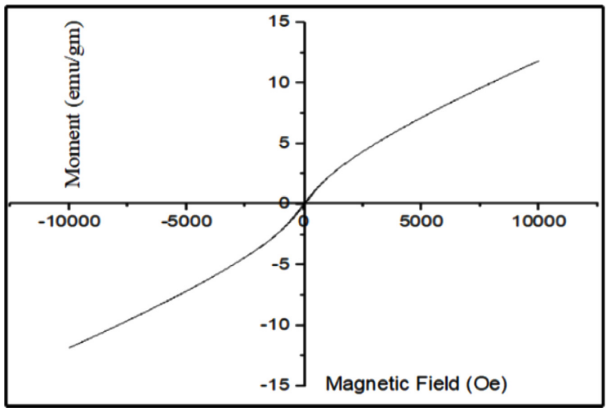

Fig. 9. Graphical representation of (M-H) curve of LS-Fe-NPs (VSM analysis).

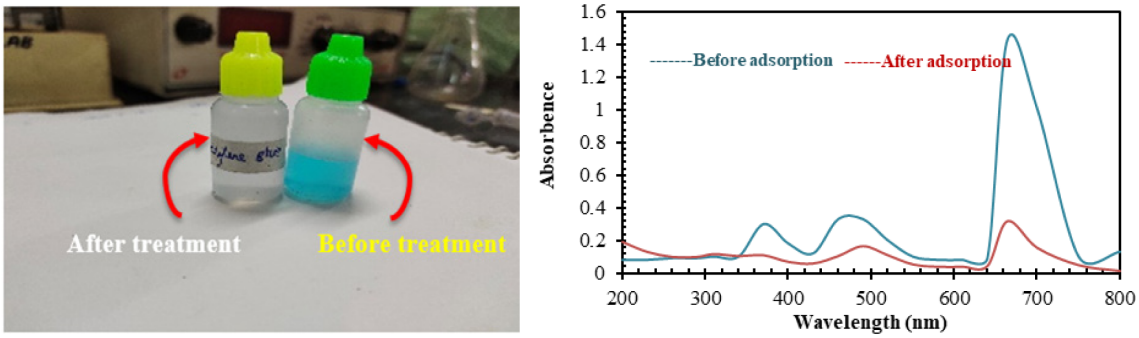

Fig. 10. (a) Photographs of MB aqueous solutions before (right), and after (left) adsorption, (b) UV-vis spectra of MB before and after adsorption in optimized conditions at wavelength of 664 nm.

as synthesis process, magnetocrystalline anisotropy, surface, and crystalline spin. The saturation magnetization value for LS-Fe-NPs, according to the hysteresis curves is 12.5 emu/g. The sample hysteresis curves showed no hysteresis loop and extremely low coercivity, indicating that nanoparticles had super-paramagnetism properties [38,39].

3-6. Dye adsorption study

The significance of contact time and adsorbent dose on the removal percentage of MB by LS-Fe-NPs by adding them into MB (100 mg/L) solution was investigated. A spectrophotometer was used to detect the concentration of MB in the supernatant at specific time intervals. The concentration of dye (MB) was identified by spectrophotometer. Fig. 10(a) shows the real photographs of MB dye before and after adsorptions, and in (b) shows UV-vis spectra, before and after adsorption of MB dye in optimized conditions at wavelength of 664 nm.

3-7. Adsorption isotherms

A proper correlation for the equilibrium curves is required to optimize the design of a sorption process. The initial dye concentrations ranged from 100 mg/L to 500 mg/L, with a nanoparticle concentration of 8 g/L remaining constant as shown in Fig. 11. To test the sorption capacity of produced LS-Fe-NPs, they were subjected to MB as an adsorbent. The Langmuir adsorption isotherm, Freundlich adsorption isotherm, and Temkin adsorption isotherms were used as model equilibrium adsorption isotherms. The Langmuir isotherm describes the adsorbents' monolayer surface coverage, whereas the Freundlich isotherm describes multilayer adsorption. The linear form of Langmuir isotherm equation is Eq. 3:

$$\frac{C_e}{q_e} = \frac{C_e}{q_m} + \frac{1}{K_L q_m} \tag{3}$$

where, q_m = maximum adsorption capacity of MB in mg/g

K_L = Langmuir constant in L/mg

Evaluation of the separation factor (R_L) determines the feasibility of the adsorption process. It can be calculated using Eq. (4):

$$R_L = \frac{1}{1 + K_L \cdot C_i} \tag{4}$$

The isotherm is considered to be linear if $R_L = 1$, favourable if $0 < R_L < 1$, unfavorable if $R_L > 1$ and if $R_L = 0$ indicates irreversible process

Freundlich isotherm model is represented in Eq. (5):

$$\log q_e = \left(\frac{1}{n}\right) \log C_e + \log K_F \tag{5}$$

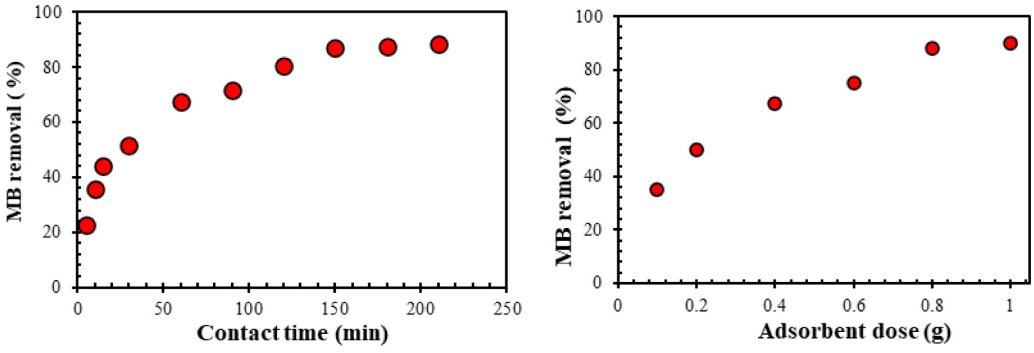

Fig. 11. Influence of process parameters: (a) Contact time, min and (b) Adsorbent dose, g for adsorption of MB dye at initial concentration of 100 mg/L, pH value 6, volume of 100 ml and temperature of 25 ℃, respectively.

Table 1. Parameters for the Langmuir, Freundlich and Temkin models of MB dye adsorption

	Langmuir Isotherm			Freundlich Isotherm			Temkin Isotherm		
Parameter	q_m	K_L	R^2	K_F	(1/n)	R^2	A_T	b_T	R^2
Value	398.406	0.011	0.966	15.001	0.562	0.991	0.084	101.951	0.954

where, n = degree of heterogeneity on the adsorbent's surface

K_F = Freundlich constant in *mg/g*.

For a favorable adsorption process, $(1/n) < 1$.

Temkin isotherm model is shown in Eq. (6):

$$q_e = \left(\frac{RT}{b_T}\right)\ln A_T + \left(\frac{RT}{b_T}\right)\ln C_e \quad (6)$$

where, A_T = equilibrium binding constant (*L/g*)

b_T = heat of adsorption.

The R^2 values derived from Freundlich isotherm model ($R^2 > 0.991$) indicated its goodness of fit than both Langmuir isotherm ($R^2 > 0.966$) and Temkin isotherm ($R^2 > 0.954$) as represented in Table 1 and Fig. 12. This revealed that multilayered (heterogeneous) adsorption as the effective mechanism for removing MB dye.

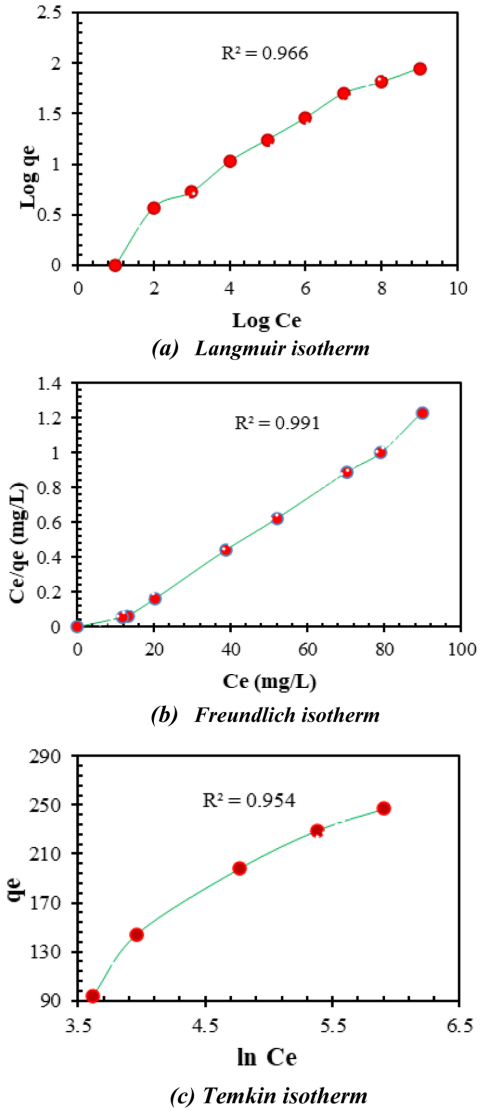

Fig. 12. Adsorption isotherms curve of (a) Langmuir isotherm, (b) Freundlich isotherm and (c) Temkin isotherm.

Table 2. Zone of inhibition of LS-Fe-NPs, against *E. coli* and Staphylococcus aureus

Sl. no.	Test	Bacteria	Size
1.	Gram positive	Staphylococcus asureus	15 mm
2.	Gram negative	Escherichia coli	13 mm

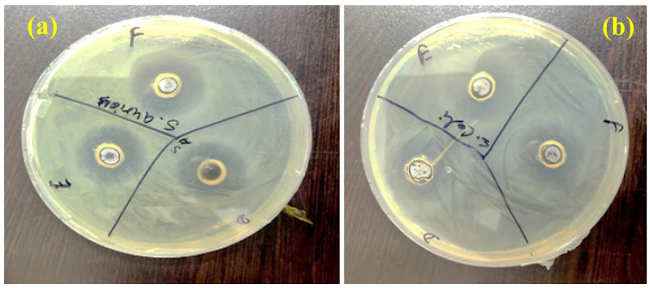

Fig. 13. Antibacterial test of (a) Antibacterial action against gram-positive bacteria (Staphylococcus aureus) and (b) Antibacterial action against gram-negative (*E. coli*).

3-8. Antibacterial action

Figs. 12(a) and (b) represent the results of a disc plate diffusion investigation to demonstrate LS-Fe-NPs antibacterial efficacy against Staphylococcus aureus (G-positive) and *E. coli* (G-negative) respectively. The area of inhibition expands as the concentration of LS-Fe-NPs rises. Moreover, the results indicate that LS-Fe-NPs are effective and superior against gram-positive bacteria Staphylococcus aureus as compared to *E. coli*. Nanoparticle activity is significantly affected by their size, which increases the LS-Fe-NPs inhibitory zone (Table 2). Metal oxides have an active role in suppressing bacterial growth by producing reactive oxygen species (ROS), which can lead to the generation of oxidative stress in bacterial cells [40,41].

4. Conclusion

The present investigation looked into the synthesis of iron oxide nanoparticles by *Lagnenaria siceraria* leaf aqueous extract (LS-Fe-NPs). The synthesized nanoparticles were obtained as spherical shape and approximately 80-100 nm in size. The magnetic hysteresis curve of the nanoparticles (LS-Fe-NPs) had no residual magnetism, which indicates that nanoparticles had super-paramagnetism properties with a saturation magnetization value of 12.5 emu/g. Moreover, LS-Fe-NPs showed 246.8 mg/g maximum adsorption capacity, with the adsorption being predominantly chemisorption. Antibacterial characteristics of the nanoparticles were also explored and it was found that LS-Fe-

NPs had a substantial bactericidal effect on G-negative (*E. coli*) and G-positive (Staphylococcus aureus) bacteria. Ultimately, this synthesized green LS-Fe-NPs could be a good candidate for several scientific aspects.

Acknowledgments

The authors express their gratitude to the Central Facility and Chemical Engineering Department, MNNIT Allahabad, India for providing the facilities to carry out the research work and analysis of the samples.

References

1. Boretti, A. and Rosa, L., "Reassessing the Projections of the World Water Development Report," *Npj Clean Water*, **2**(1), 15 (2019).
2. Gutierrez, A. M., Dziubla, T. D. and Hilt, J. Z., "Recent Advances on Iron Oxide Magnetic Nanoparticles as Sorbents of Organic Pollutants in Water and Wastewater Treatment," *Rev. on Env. Health*, **32**(1-2), 111-117(2017).
3. Agarwal, M. and Singh, K., "Heavy Metal Removal from Wastewater Using Various Adsorbents: A Review," *J. Water. Reuse and Desal.*, **7**(4), 387-419(2017).
4. Mehdipour, S., Vatanpour, V. and Kariminia, H. R., "Influence of Ion Interaction on Lead Removal by a Polyamide Nanofiltration Membrane," *Desal.*, **362**, 84-92(2015).
5. Rawat, S., Samreen, K., Nayak, A.K., Singh, J. and Koduru, J. R., "Fabrication of Iron Nanoparticles Using Parthenium: A Combinatorial Eco-innovative Approach to Eradicate Crystal Violet Dye and Phosphate from the Aqueous Environment," *Env. Nanotech. Mon. & Manag.*, **15**, 100426(2021).
6. Yang, X., Chung, E., Johnston, I., Ren, G. and Cheong, Y. K. "Exploitation of Antimicrobial Nanoparticles and Their Applications in Biomedical Engineering," *App. Sci.*, **11**(10), 4520 (2021).
7. Kouhbanani, M., Beheshtkhoo, N., Amani, A., Taghizadeh, S., Beigi, V. and Bazmandeh, A., "Green Synthesis of Iron Oxide Nanoparticles Using Artemisia Vulgaris Leaf Extract and Their Application as a Heterogeneous Fenton-like Catalyst for the Degradation of Methyl Orange," *Mat. Res. Exp.*, **5**(11), 115013 (2018).
8. Ali, A., Shah. T., Ullah, R., Zhou, P., Guo, M. and Ovais, M., "Review on Recent Progress in Magnetic Nanoparticles: Synthesis, Characterization, and Diverse Applications," *Fron. Chem.*, **9**, 2296-2646(2021).
9. Kianfar, E., Magnetic Nanoparticles in Targeted Drug Delivery: a Review," *J. Superconduct. Novel Mag.*, **34**(7), 1709-1735(2021).
10. Wang, Y., Zou, L., Qiang, Z., Jiang, J., Zhu, Z. and Ren, J., "Enhancing Targeted Cancer Treatment by Combining Hyperthermia and Radiotherapy Using Mn-Zn Ferrite Magnetic Nanoparticles," *ACS Biomat. Sci. Eng.*, **6**(6), 3550-3562(2020).
11. Qamer, S., Romli, M. H., Che-Hamzah, F., Misni, N., Joseph, N. M. S. and Al-Haj, N. A., Systematic Review on Biosynthesis of Silver Nanoparticles and Antibacterial Activities: Application and Theoretical Perspectives," *Molec.*, **26**(16), 50-57(2021).
12. Lee, N. and Hyeon, T., "Designed Synthesis of Uniformly Sized Iron Oxide Nanoparticles for Efficient Magnetic Resonance Imaging Contrast Agents," *Chem. Soc. Rev.*, **41**(7), 2575-2589(2012).
13. Mehnaz, R., Rabbi, M., Ara, T., Elaissari, A., Ahmad, H. and Hossain, Md., "Vancomycin Conjugated Iron Oxide Nanoparticles for Magnetic Targeting and Efficient Capture of Gram-positive and Gram-negative Bacteria," *RSC Adv.*, **11**, 36319-36328(2021).
14. Hilger, I., Hiergeist, R., Hergt, R., Winnefeld, K., Schubert, H. and Kaiser, W. A., "Thermal Ablation of Tumors Using Magnetic Nanoparticles," *Investigative Radiology*, **37**(10), 580-586(2002).
15. Rodrigues, C. R., García, L. R., Baptista, P. V. and Fernandes, A. R., "Gene Therapy in Cancer Treatment: Why Go Nano?," *Pharmaceutics*, **12**(3), 233(2020).
16. Nile, S. H., Baskar, V., Selvaraj, D., Nile, A., Xiao, J. and Kai, G., "Nanotechnologies in Food Science: Applications, Recent Trends, and Future Perspectives," *Nano-Micro Lett.*, **12**(1), 45 (2020).
17. Saili, K., Rachana, Y., Shuana, M. and Balaprasad, A., "A Review on Green Synthesis and Applications of Iron Oxide Nanoparticles," *J. Nanoscie. Nanotech.*, **21**(12), 6168-6182(2021).
18. Pradeep, T. and Anshup., "Noble Metal Nanoparticles for Water Purification: A Critical Review," *Thin Solid Films*, **517**(24), 6441-6478(2009).
19. Sánchez-López, E., Gomes, D., Esteruelas, G., Bonilla, L., Lopez-Machado, A. L. and Galindo, R., "Metal-Based Nanoparticles as Antimicrobial Agents: An Overview," *Nanomat.*, **10**(2), 1-39(2020).
20. Gudkov, S. V., Burmistrov, D. E., Serov, D. A., Rebezov, M. B., Semenova, A. A. and Lisitsyn, A. B., "Metal-Based Nanoparticles as Antimicrobial Agents: An Overview," *Antibiot.*, **10**(7), 1-23(2021).
21. Hyunhee, S. and Yul, R., "Mixed Contaminants Removal Efficiency Using Bio-FeS Nanoparticles," *J. Nanosci. Nanotech.,* **18**(2), 1127-1130(2018).
22. Urnukhsaikhan, E., Bold, B. E., Gunbileg, A., Sukhbaatar, N. and Mishig-Ochir, T., "Antibacterial Activity and Characteristics of Silver Nanoparticles Biosynthesized from Carduus Crispus," *Sci. Rep.*, **11**(1), 1-12(2021).
23. Abbas, A. and Razieh, M., "Adsorptive Removal of Congo Red, a Carcinogenic Textile Dye, from Aqueous Solutions by Maghemite Nanoparticles," *J. Haz. Mat.*, **174**(1-3), 398-403(2010).
24. Machado, S., Pinto, S. L., Grosso, J. P., Nouws, H. P., Albergaria, J. T. and Delerue-Matos, C., "Green Production of Zero-valent Iron Nanoparticles Using Tree Leaf Extracts," *Sci. Tot. Env.*, **445**, 1-8(2013).
25. Saif, S., Tahir, A. and Chen, Y., "Green Synthesis of Iron Nanoparticles and Their Environmental Applications and Implications," *Nanomat.*, **6**(11), 1-26(2016).
26. Kaur, K. and Sidhu, A. K., "Green Synthesis: An Eco-friendly Route for the Synthesis of Iron Oxide Nanoparticles," *Fron. in Nanotech.*, **3**, 2673-3013(2021).
27. Devatha, C. P., Thalla, A. K. and Katte, S. Y., "Green Synthesis of Iron Nanoparticles Using Different Leaf Extracts for Treatment of Domestic Waste Water," *J.Clean. Prod.*, **139**, 1425-1435 (2016).
28. Devatha, C. P., Thalla, A. K. and Katte, S. Y., "Green Synthesis of Iron Nanoparticles Using Different Leaf Extracts for Treat-

ment of Domestic Waste Water," *J. Clean. Prod.*, **139**, 1425-1435 (2016).
29. Kanagasubbulakshmi, S. and Kadirvelu, K., "Green Synthesis of Iron Oxide Nanoparticles Using Lagenaria Siceraria and Evaluation of Its Antimicrobial Activity," *Def. Life Sci.*, **2**(4), 422(2017).
30. Wang, T., Lin, J., Chen, Z., Megharaj, M. and Naidu, R., "Green Synthesized Iron Nanoparticles by Green Tea and Eucalyptus Leaves Extracts Used For Removal of Nitrate in Aqueous Solution," *J. Clean. Prod.*, **83**, 413-419(2014).
31. Hongtao, G., Miaomiao, K., Hui, S., Tian, F., Dongmei, D. Fenghua, L. and Chongdian, S., *J. Nanoscie and Nanotech.*, **18**(2), 1034-1042(2018).
32. Lebogang, K. S., Tshepiso, M., Samuel, A. O. and Indra, B., "Green Synthesis of Iron Nanoparticles Using Moringa Oleifera Extracts and Their Applications: Removal of Nitrate from Water and Antibacterial Activity Against Escherichia coli," *Molec. Liq.*, **256**, 296-304(2018).
33. Zhang, Q., Yang, X. and Guan, J., "Applications of Magnetic Nanomaterials in Heterogeneous Catalysis," *ACS App. Nano Mat.*, **2**(8), 4681-4697(2019).
34. El-Shahaw, M. S., Hamza, A., Bahaffi, S. O., Al-Sibaai, A. A. and Abduljabbar, T. N., "Retention Profile and Selective Separation of Trace Concentrations of Phenols from Water onto Iron (III) Physically Loaded Polyurethane Foam Solid Sorbent: Kinetics and Thermodynamic Study Food Chem," *Chromatog. & Sep. Tech.*, **134**, 2268-2275(2012).
35. Karpagavinayagam, P. and Vedhi, C., "Green Synthesis of Iron Oxide Nanoparticles Using Avicennia Marina Flower Extract," *Vacuum*, **160**, 286-292(2018).
36. Bibi, I., Nazar, N., Iqbal, M., Kamal, S., Nawaz, H. and Nouren, S., "Green and Eco-friendly Synthesis of Cobalt-oxide Nanoparticle: Characterization and Photo-catalytic Activity," *Adv. Powder Tech.*, **28**(10), 2035-2043(2017).
37. Somchaidee, P. and Tedsree, K., "Green Synthesis of High Dispersion and Narrow Size Distribution of Zero-valent Iron Nanoparticles Using Guava Leaf (Psidium guajava L) Extract," *Adv. in Nat. Sci: Nanosci. and Nanotech*., **9**(3), 035006(2018).
38. Brajesh, K., Kumari, S., Luis, C. and Alexis, D., "Biogenic Synthesis of Iron Oxide Nanoparticles for 2-arylbenzimidazole Fabrication," *J. Saudi. Chem. Soc.*, **18**(4), 364-369(2014).
39. Shu, H. Y., Chang, M. C., Yu, H. H. and Chen, W. H., "Reduction of An Azo Dye Acid Black 24 Solution Using Synthesized Nanoscale Zerovalent Iron Particles," *J. Coll. Interf. Sci.*, **314**(1), 89-97(2007).
40. Guo-Xiang, R., Zhi-Xiang, L., Zhong-Jun, P., Shuang-Long, Z. and Peng, D., "Immobilization of Cellulase onto Amino and Graphene Oxide Functionalized Magnetic $Fe_2O_3/Fe_3O_4@SiO_2$ Nanocomposites," *J. Nanoscie. Nanotech.*, **21**(9), 4749-4757 (2021).
41. Harish, K., Kumar, G. A., Ankur, G., Jin-Won, P. and Sanjeev, M., "Facile Synthesis of SiO_2/CMC/Ag Hybrids Derived from Waste Biomass (Sugarcane Bagasse) Having Special Medical Application," *J. Nanoscie. Nanotech*., **20**(10), 6413-6421(2020).

Authors

Kirti: Department of Chemical Engineering, Motilal Nehru National Institute of Technology, Allahabad, India; kirtichemical88@gmail.com

Suantak Kamsonlian: Department of Chemical Engineering, Motilal Nehru National Institute of Technology, Allahabad, India; suantakk@mnnit.ac.in

Vishnu Agarwal: Department of Biotechnology, Motilal Nehru National Institute of Technology, Allahabad, India; vishnua@mnnit.ac.in

Ankur Gaur: Department of Chemical Engineering, Motilal Nehru National Institute of Technology, Allahabad, India; ankur@mnnit.ac.in

Jin-Won Park: Department of Chemical Engineering, Yonsei University, Seoul, Korea; jwpark@yonsei.ac.kr